International Journal of Coal Geology 277 (2023) 104340

Contents lists available at ScienceDirect

International Journal of Coal Geology

journal homepage: www.elsevier.com/locate/coal

Subcritical CO_2 adsorption on geomaterials of coal-bearing strata in the context of geological carbon sequestration

Maram Almolliyeh [a,*], Snehasis Tripathy [a], Sivachidambaram Sadasivam [a], Shakil Masum [a], Sara Edwards Rassner [b], Andy Mitchell [c], Hywel Rhys Thomas [a]

[a] Geoenvironmental Research Centre (GRC), School of Engineering, Cardiff University, The Queen's Buildings, The Parade, Cardiff CF24 3AA, United Kingdom
[b] Department of Life Sciences, IBERS Building, Aberystwyth University, Aberystwyth SY23 3FG, United Kingdom
[c] Department of Geography and Earth Sciences, Llandinam Building, Aberystwyth University, Aberystwyth SY23 3DB, United Kingdom

ARTICLE INFO

Keywords:
CO2 Adsorption
Coal seam
Caprock
Biofilm
Water
CO2 sequestration in geological formations
CCS
CCUS

ABSTRACT

This paper explores the adsorption behaviour of geomaterials in the framework of CO_2 sequestration in shallow level coal seams. Manometric adsorption experiments were carried out on two anthracite coal samples, two rock samples from East Irish Sea, MX80-bentonite, Speswhite kaolinite, dry, wet and biofilm-laden (*Bascillus mojavensis*-laden) sand at subcritical pressure range (up to 6.4 MPa) of isothermal condition at 298.15 K. The experiments were aimed to investigate the influence of the biogeological conditions of coal and caprock constitutions on CO_2 adsorption. At lower pressures, the moisture had an influence on the CO_2 adsorption on coal resulted in reduced adsorption capacity. At elevated pressures, the volume expulsion behaviour and coal-water interaction had an influence on the adsorption capacities of moist coal sample and resulted in comparable adsorption capacities to dry sample. The disparity in the adsorption capacities between the wet powdered and wet intact core samples showed that the results obtained with powder samples may not reflect the field conditions. Wet conditions and *Bascillus mojavensis* bacteria influenced the adsorption capacity of sand and showed CO_2 chemisorption capacity. The desorption isotherm pattern of wet and biofilm sand showed that the CO_2 was continuously adsorbed independent of the gas phase pressure. Among the clay minerals, bentonite had greater affinity towards CO_2. Despite the fact that the adsorption capacity of the cap rock is smaller than that of the coal samples, the experimental investigation with constituents of the cap rock provides insights into the effect of biogeological conditions of coal and rock sample constituents on CO_2 storage in coal seams.

1. Introduction

CO_2 adsorption capacity and kinetics are associated with coal rank, moisture content, swelling characteristics, porosity, temperature, and operating pressures (White et al., 2005). The biogeological conditions of coal and adjacent caprock have also had an impact on the coal seams' CO_2 sequestration potential. The adsorption capacity was suppressed in the presence of moisture for low-rank coals, and the experimental results showed that CO_2 prefers the H_2O sites (competing with water) (Day et al., 2008; Ozdemir and Schroeder, 2009; Pone et al., 2009). There is a scarcity of data on the adsorption of CO_2 on wet intact coal samples apart from the studies conducted on constructed coal samples or moisture equilibrated powdered samples (Zhang et al., 2019; Wang et al., 2017), which may not represent the field conditions. Water molecules form hydrogen bonds with the functional groups on the coal surface. The higher the amount of polar functional groups such as OH^-, carboxyl (COOH), methoxy (-OCH3), and carboxyl (C=O) groups present in coal, the more hydrophilic it is (Mahajan and Walker, 1971; Allardice and Evans, 1971; Nishino, 2001; Qi and LeVan, 2005; Miura et al., 2001; Kadioğlu and Varamaz, 2003). The carbon-containing groups mentioned above decompose and increase the fixed carbon content of high-rank anthracite coal while decreasing its hydrophilicity (Stach et al., 1982; Allardice and Evans, 1971; Murata et al., 2000; Allardice et al., 2003; Charrière and Behra, 2010), which would reflect on the CO_2 adsorption capacity. The CO_2 can interact with adsorbed water on coal and raise the carbonic acid content, dissolve alkaline (Ca, Na, K, and Mg-containing) minerals from the coal, and induce CO_2 mineralisation as $CaCO_3$ (Massarotto et al., 2010).

The rock strata above the coal seam serve as a caprock system for the CO_2 reservoir in the coal seam. Testing the integrity of the caprock and

* Corresponding author.
E-mail address: almolliyehm1@cardiff.ac.uk (M. Almolliyeh).

https://doi.org/10.1016/j.coal.2023.104340
Received 9 March 2023; Received in revised form 20 August 2023; Accepted 20 August 2023
Available online 22 August 2023

associated minerals will be necessary for mitigating the level of risk in CO_2 injection in coal seams. The CO_2 gas can permeate, trapped in the porous structure of the rock, chemically interact with water, and adsorb on the rock minerals. CO_2 can be captured in the caprock system through a variety of mechanisms, including structural trapping, residual trapping, solubility trapping, mineral trapping, and adsorption (Depaolo and Cole, 2013). Sandstone and mudstone formations dominate the rock strata above the coal seams. Sandstone is primarily composed of quartz, with trace amounts of clays (e.g., kaolinite and bentonite). In consequence, studying the CO_2 adsorption capacity of sand (quartz) and clays would advance our understanding of CO_2 sequestration in un-minable coal seams (Wang et al., 2003; Yang and Yang, 2011; Botan et al., 2010; McGrail et al., 2009; Kwak et al., 2011; Loring et al., 2011; Shao et al., 2011; Tokunaga and Wan, 2013; Chen and Lu, 2015; Jeon et al., 2014; Wensink et al., 2000; Rahaman et al., 2008; Malani and Ayappa, 2009; Kerisit et al., 2012).

Microbial activities have also been reported in rock strata and influence the fate and transport mechanism of CO_2 at potential geological carbon sequestration (GCS) sites (Morozova et al., 2010; Lavalleur and Colwell, 2013; Peet et al., 2015). Supercritical CO_2 is used as a disinfectant against microorganisms (Dai et al., 2016). Yet, biofilms formed by *Bacillus mojavensis* bacteria are able to withstand supercritical CO_2. *Bacillus mojavensis* is a commonly found microorganism in the sandstone cores from coal field and can withstand high-pressure conditions (Kamihira et al., 1987; Enomoto et al., 1997; Zhang et al., 2006; Mitchell et al., 2009). Previous studies indicate that *Bacillus mojavensis* are capable of resisting CO_2 exposure than many other bacteria (Mitchell et al., 2008). This finding highlights the importance of conducting additional experiments on *Bacillus mojavensis* biofilm-loaded sand samples at various pressure ranges to examine the impact of the biogeochemical nature of the rock strata on CO_2 adsorption capacity.

In this work, two high-rank anthracite coals, two rock samples from East Irish Sea, dry, wet and biofilm loaded sand, kaolinite and bentonite samples were investigated for their CO_2 adsorption capacity to improve our understanding of CO_2 adsorption in coal seams under field conditions.

2. Materials and methods

2.1. Materials

The adsorption experiments were carried out on two coal samples and caprock constituents. The two anthracite coal samples were obtained from the Aberpergwm coal mine (51°44′28.8”N 3°38′36.0”W), Wales, UK and referred as to 9 ft. AB and 18 ft. AB with natural water content of 0.91% and 0.78%, respectively. Commercially available MX80 bentonite, Speswhite kaolinite and sand samples were used in the CO_2 adsorption experiments. The supplementary section contains x-ray diffraction (XRD) mineralogical identifications of clay minerals. The British Geological Survey (BGS) provided the two rock core samples from the East Irish Sea that measured 2.54 cm in diameter referred as to R1 and R2. The Proximate and ultimate analysis of the coal samples and the properties of geomaterials have been provided in Table 1. Fig. 1 shows the representative examples of the materials used in the study.

2.2. Geological settings and properties of the coal and rock samples

The 9 ft. coal samples were procured from the depth of 550 and the 18 ft. coal seam is located at 500 m. The strata consist of sandstone, siltstone, mudstone, and coal seams from the Carboniferous period and dip between 25 and 45° to the south and southwest. The detailed geological settings and baseline geochemistry of the coal seams provided by Sadasivam et al. (2019). The properties of coal seams are found in Table 1.

The X-ray diffraction (XRD) patterns of East Irish Sea rock samples collected from different depths are displayed in Fig. 2. The X-ray diffraction patterns clearly show that The rock samples are primarily composed of quartz (SiO_2, primary peaks $2\Theta = 26.64°$, 20.86° and 50.13°), ankerite (dolomite with iron substitution, Ca $(Mg_{0.67}Fe_{0.3})(CO_3)_2$, primary peak $2\Theta = 30.81°$) and showed peaks attributes for halite (primary peaks at $2\Theta = 31.69°$, 45.45°), kaolinite (major peak at $2\Theta = 12.28°$) and orthoclase (major peak at $2\Theta = 25.65°$).

The chemical composition of the rock samples obtained from an x-ray fluorescence spectrometer is shown in Table 2. The compositions of major oxides (SiO_2, Al_2O_3, CaO, FeO, K_2O, and TiO_2) confirm the mineralogical identification of the rock samples by XRD. Quartz (SiO_2 = 50%–89% SiO_2) is the predominant constituent of the rock samples, followed by iron (1.3% to 6.6%) and calcium (3.4%–25%) containing minerals (Table 2).

Table 1
Proximate and ultimate analysis of the coal samples from 9 ft. and 18 ft. Aberpergwm.

Analytical		18 ft. Aberpergwm Coal	9 ft. Aberpergwm Coal
Proximate analysis			
Water Content	%	0.78	0.91
Ash Content	mass	1.38	4.62
Volatiles content	%	5.08	5.73
	mass		
	%		
	mass		
Calorimetry			
High calorific value	Mj/kg	35.04	35.60
Low calorific value	Mj/kg	34.30	32.89
Ultimate analysis			
Total Carbon	%	92.05	89.5
Total sulphur	mass	0.73	0.87
Sulphur combustion	%	0.01	0.25
Sulphur after full	mass		
combustion	%	0.72	0.62
Combustible sulphur	mass	92.05	89.5
Total hydrogen	%	3.31	3.16
Nitrogen	mass	1.27	1.31
Oxygen		0.5	0.33
	%		
	mass		
	%		
	mass		
	%		
	mass		
	%		
	mass		
Petrography			
Vitrinite reflectance	% Vol	2.72	2.84
Vitrinite content	% Vol	86	86
Liptynite (egsynite)	% Vol	0	0
Inertynite	% Vol	14	14
Mineral matter content	% Vol	0	0
As received			
Transient moisture	%	0.84	0.65
content	mass	1.61	1.56
Total moisture	%	1.37	4.59
Ash content	mass	5.04	5.69
Volatile matter content	%	0.72	0.86
Total sulphur content	mass	33.99	32.66
Low calorific value	%		
	mass		
	%		
	mass		
	Mj/kg		
Dry state			
Ash	%	1.39	4.66
Total sulphur	mass	0.74	0.88
	%		
	mass		
Daf state			
Volatile matter content	%	5.19	6.07
High calorific value	mass	33.82	35.57
	%		
	mass		

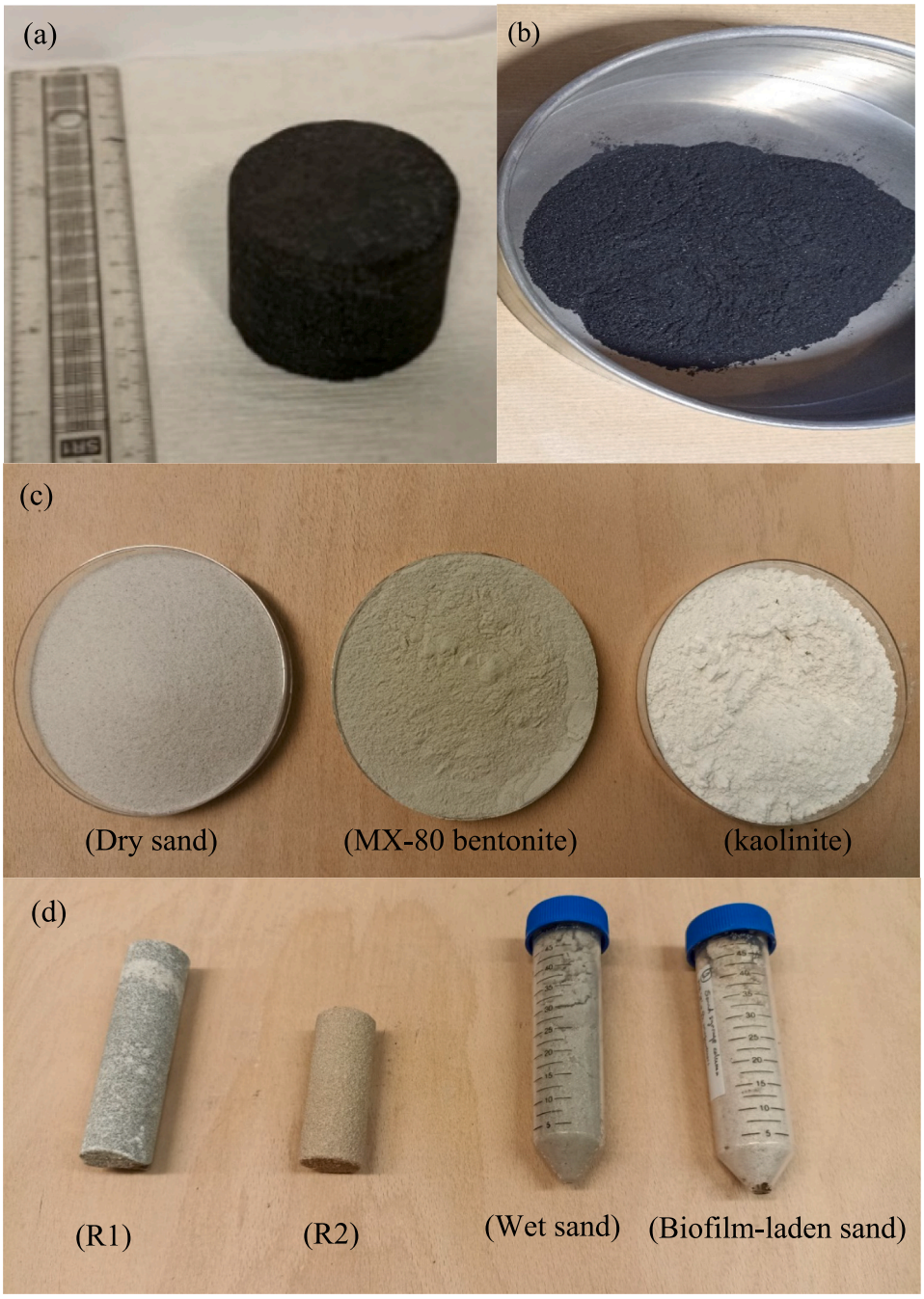

Fig. 1. (a) Intact coal core, (b) powdered coal, (c) dry sand, MX-80 m bentonite and kaolinite and (d) East Irish Sea rock samples (R1 and R2) and wet sand and biofilm loaded sand.

Clearly, the overburden would contain a range of minerals, particularly carbonate minerals (Fig. 2; Table 2), which are ubiquitous in sedimentary rocks and react more rapidly than silicates. Ankerite (which contains Fe) is the most common carbonate mineral after calcite, dolomite, and siderite. CO_2-laden groundwater can dissolve iron and calcium-containing minerals such as ankerite (Doner and Lynn, 1989).

2.3. Methods

2.3.1. Preparation of wet intact and powdered coal samples

Intact samples were drilled from the large coal blocks using a core drill with a 5 cm internal diameter diamond core bit for the adsorption experiments. The core samples were saturated with water using an oedometer to prepare moist coal samples (Fig. 3). The core samples were left in the cells for minimum of 21 days to attain saturation equilibrium under 1 MPa pressure. The saturation pressure was chosen to maintain the water pressure above 0.1 MPa to saturate the microfractures (Zhang et al., 2022). Moist powder coal samples were prepared as described in previous literatures (ASTM D1412–072007; Krooss et al., 2002; Wang et al., 2017, Mukherjee and Misra, 2018). The resulted water content of intact 9 ft. AB sample was about 2.34%, intact 18 ft. AB was about 4.07% and powder samples of 18 ft. AB was about 1.2%. Adsorption experiments were conducted on samples of water equilibrated and samples with natural water content to compare the effect of water on CO_2 adsorption.

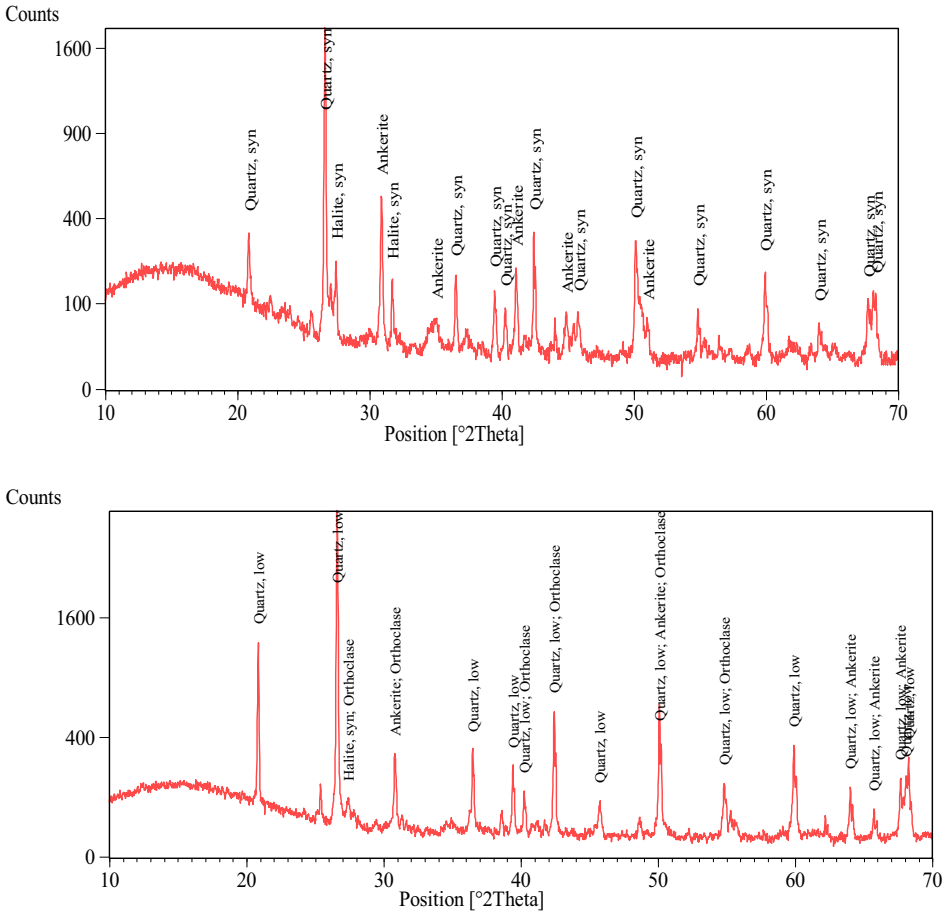

Fig. 2. X-ray diffraction patterns of X-ray diffraction (XRD) patterns of powdered East Irish Sea rock samples (depth of the samples indicated): (a) R1; 4064 m to 4065 m, (b) R2; 8379 m to 8379.57 m.

Table 2
Chemical composition of the rock samples (values are within ±5% error).

Rock sample core number (depth in m)/ % composition	SiO_2%	Al_2O_3%	CaO %	FeO %	K_2O %	TiO_2%	% mass
R1 (4064 to 4065 m)	63.26	1.17	20.25	4.92	9.05	1.33	99.98
R2 (6499 to 6500 m)	80.73	0.42	9.54	1.18	1.67	0.34	93.87

2.3.2. Dry, Wet sand and biofilm-laden (Bacillus mojavensis) sand sample preparation

The sand samples were dried at 105 °C for 24 h and referred as to dry sand. To avoid microbial growth, a dried portion of sand was equilibrated with water and stored in a freezer. One day prior to the adsorption tests, the samples were transferred to a refrigerator. These samples were designated as wet sand samples.

Bacillus mojavensis grown in Nutrient Broth E was added to the sand samples. The biofilm loading was developed in syringe sand columns (Fig. 4). Each sand column was filled with 50 mL of fine sand. Prior to biofilm loading, the sand was heated to 150 °C for 1 h in order to kill any bacteria present in the sand. The assembly is designed for single-pass flow of medium, nutrient solution, and deionised water (Milli-Q Water). The fluids were introduced into the system using a Watson-Marlow pump 205S multichannel pump (8 channels). To flush the system, autoclaved deionised water was run through the sand columns overnight.

Bacillus mojavensis starter culture was prepared and left to grow overnight at 30 °C (optimum temperature to grow the culture). To grow the biofilm, six syringe columns were prepared, one of which served as a control. Four millilitres of the prepared *Bacillus mojavensis* culture was injected and pushed into the sand column at a rate of 4.17 mL/min. The pump flow rate was then reduced to 0.056 mL/min to pump 60 mL of fluid media to allow the bacteria to attach and form a biofilm on the sand.

Following biofilm loading, the liquid was drained and sand portions

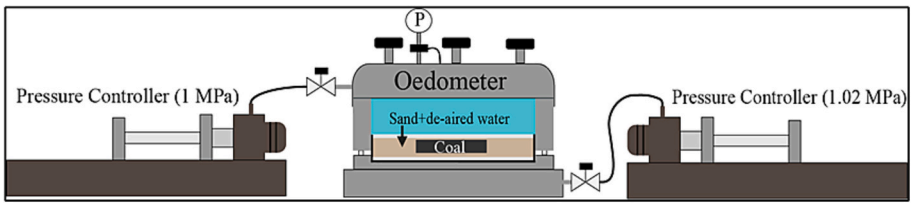

Fig. 3. Schematic for intact coal saturation procedure using oedometer.

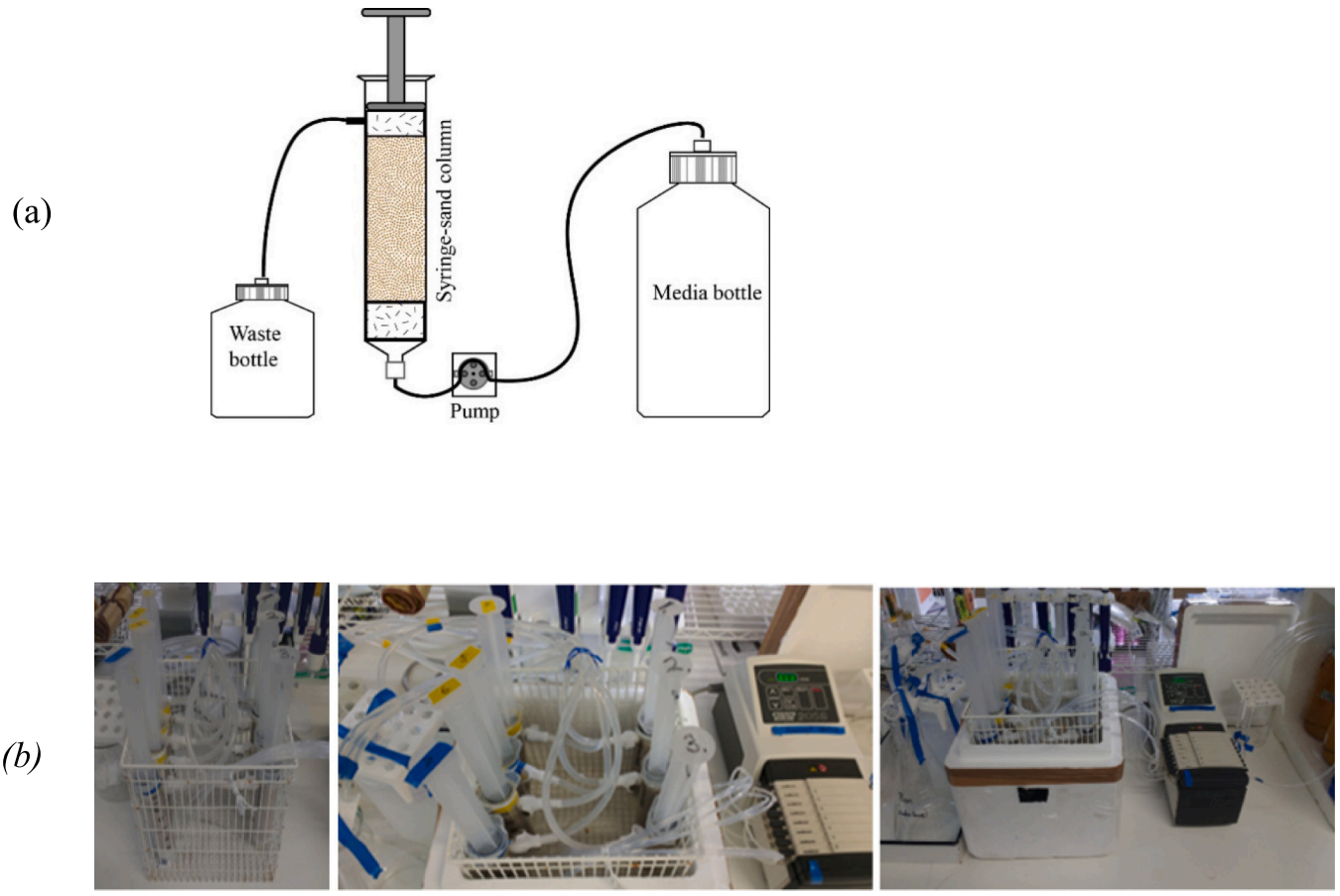

Fig. 4. (a) Schematic and (b) Photographs of the syringe sand columns with single-pass flow system for loading biofilm (*Bacillus mojavensis* grown in Nutrient Broth E).

were transferred to sterile 50 mL Falcon tubes and stored in a freezer prior to adsorption experiments. The samples were taken out of the freezer 24 h prior to the adsorption experiments.

2.3.3. Adsorption experiment

Fig. 5 illustrates a simplified schematic of the volumetric/manometric adsorption experimental setup. The apparatus is made up of a gas supply, an adsorption apparatus with a reference cell (RC), a sample cell

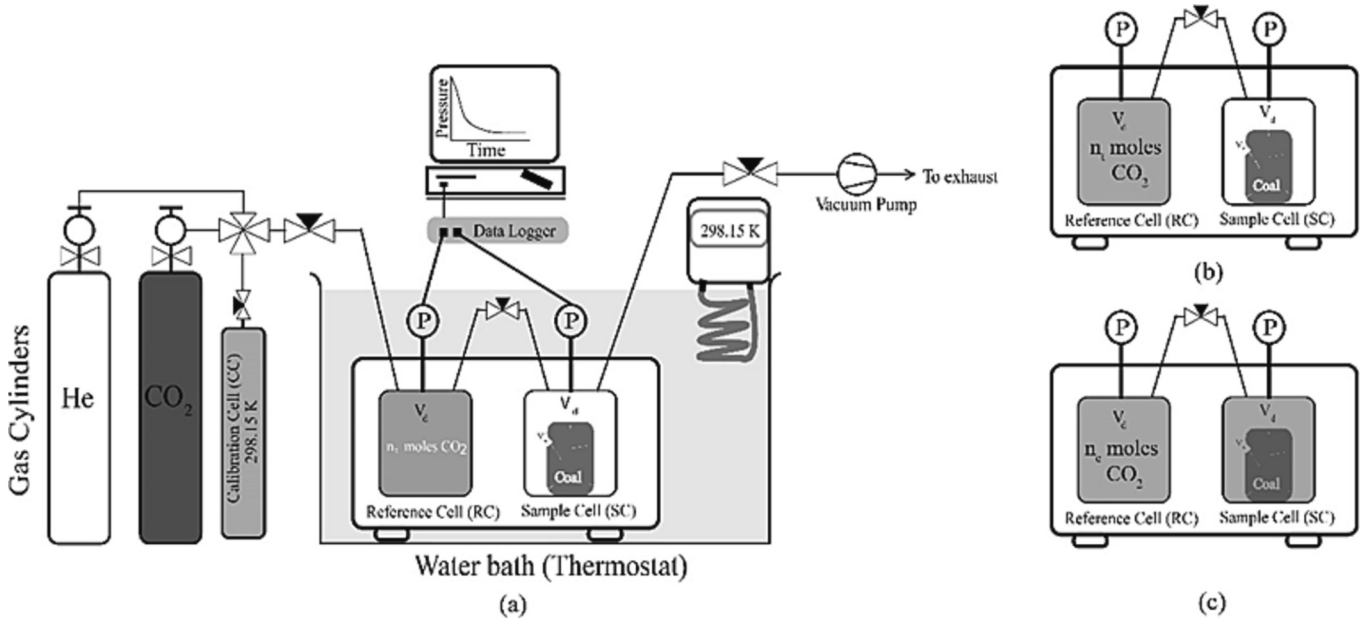

Fig. 5. (a) Schematic illustration of the volumetric/manometric experimental setup, (b) known amount of CO_2 prepared in Reference Cell (RC) and (c) CO_2 expanded into Sample cell (SC) and allowed to reach equilibrium.

(SC), and pressure transducers for measuring the gas phase pressure in the adsorption cell. The entire setup is contained within a thermostat (water bath) to maintain a constant temperature of 298.15 K (Fig. 5). A known mass (m_s) of adsorbent is placed in the sample cell that has been vacuum degassed to remove any trapped gas in the sample. A known quantity (n_t) of gas (CO_2) is injected into the RC, expanded into the SC, and adsorbed on the adsorbent. Not all gas molecules are adsorbed and a small amount of gas remains in the gas phase at equilibrium. The amount adsorbed is the difference between the amount of gas in the gas phase (n_e) and the known amount (n_t) of gas (CO_2) injected into the RC (Keller and Staudt, 2005; Myers and Monson, 2014). The experiments were carried out at pressure step-up stages ranges from 0.5 MPa to 6.5 MPa at isothermal conditions (298.15 K). The adsorbed amount is arithmatically added to calculate the cumulative amount of CO_2 adsorbed at each pressure step up stages. The desorption pressure step-down experiments were carrried out to claculate the amount of CO_2 released from the adsorbed phase. The amount adsorbed during the adsorption and desorption experiments were calculated for each gas equilibrium stages as follow.

$$n_t^{CO_2} = \frac{p^{CO_2}}{RTZ_{(p,v)}} v_d \tag{1}$$

$$n_e^{CO_2} = \frac{p_{eq}^{CO_2}}{RTZ_{(p,v)}} v_d \tag{2}$$

$$n_{ad}^{CO_2} = \frac{n_t^{CO_2} - n_e^{CO_2}}{m_s} \text{ adsorption}; n_{de}^{CO_2} = \frac{n_e^{CO_2} - n_e^{CO_2}}{m_s} \text{ desorption} \tag{3}$$

where $n_t^{CO_2}$ is the known amount present in the gas phase at the beginning of the adsorption experiment (mol), $n_e^{CO_2}$ is number of moles of CO_2 at equilibrium stage (mol), $n_{ad/de}^{CO_2}$ is amount of CO_2 adsorbed over known mass of adsorbent (mol/kg) during adsorption/desorption, v_d is void volume available for gas, (v_d is sample cell volume with sample loaded + reference cell volume), p^{CO_2} is pressure of CO_2 at the beginning of each experimental stage, $p_{eq}^{CO_2}$ is equilibrium pressure of CO_2 (Pa) measured in RC + SC, R is gas constant 8.314 (J/mol.K), T is temperature (298.15 K) and *Z*-is compressibility factor of CO_2. The compressibility factor (Z) was determined using the Peng-Robinson equation of state (Elliott and Lira, 2012). The experimental results were fit into isotherm models (Langmuir and Brunauer-Emmer-Teller [BET]) and psudeo-first-order (PFO) and psudeo second-order (PSO) kinetic models (Langmuir, 1915, 1916, 1917, 1918; Brunauer et al., 1938; Guo et al., 2017; Hu et al., 2020).

To substantiate the influence of the physical and chemical nature of

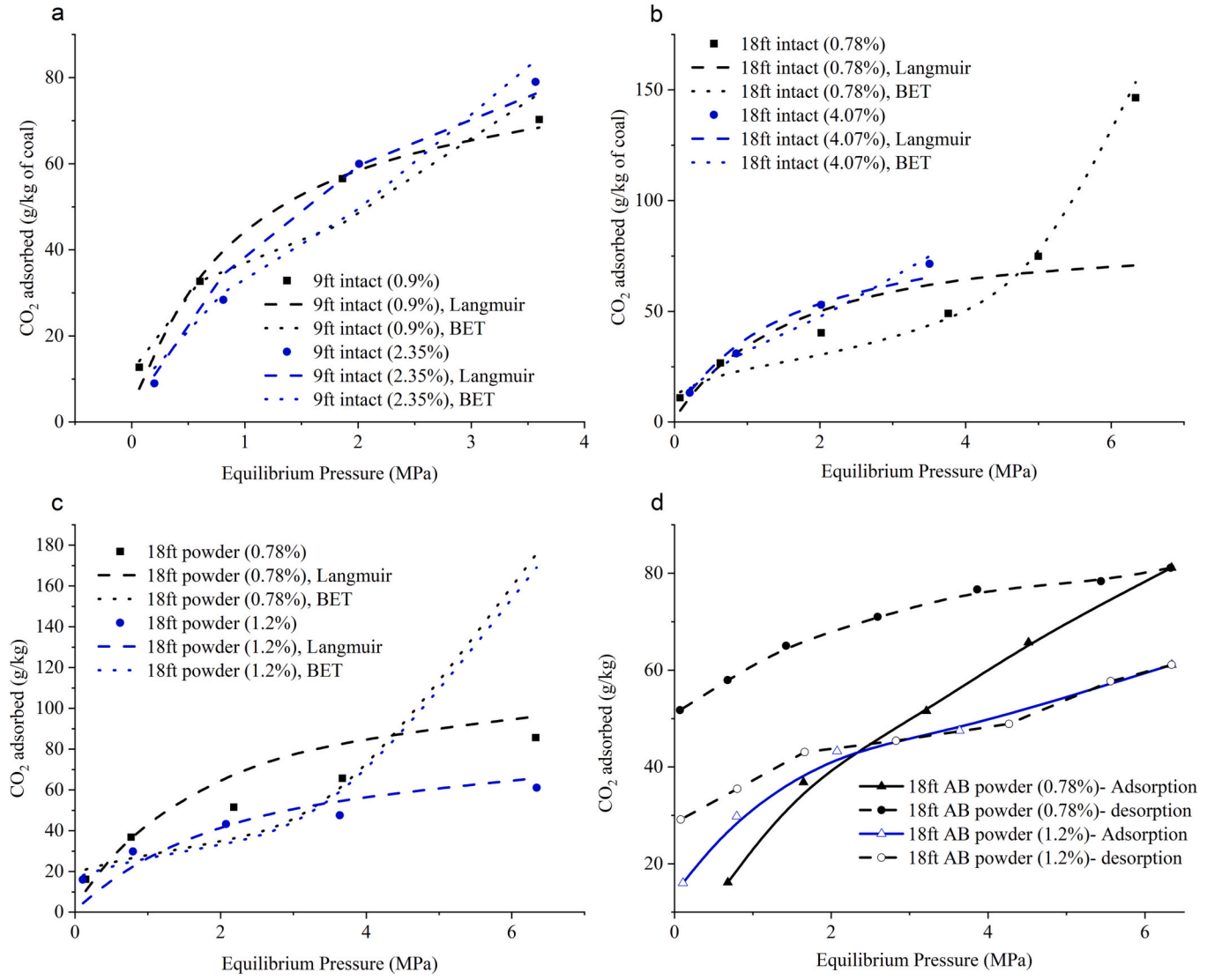

Fig. 6. Adsorption isotherms of (a) 9 ft. AB (0.9%, 2.35% water content), (b) 18 ft. AB (0.78% and 4.07% water content), (c) powdered 18 ft. AB (0.78% and 1.2%) and (d) adsorption-desorption isotherms of 18 ft. AB powder (0.78% and 1.2%).

water on adsorption of coal samples, water retention characteristic curves, pH buffering of coal and evidence of the presence of bioflim on coal were also obtained. Procedure of these experiments are detailed in the supplimentary section.

3. Results and discussions

3.1. CO_2 adsorption on moist coal samples

The CO_2 adsorption isotherms of intact samples of 9 ft. AB coal with water content of 0.91% and 2.35%, respectively, are depicted in Fig. 6a. When the adsorption isotherms were compared, a marginal increase in CO_2 adsorption was observed for the sample with greater moisture content at the higher-pressure range. At an equilibrium pressure of 3.6 MPa, adsorption capacity of the sample with 2.35% water content was about 79 g/kg (1.8 mol CO_2/kg), whereas the sample with lower moisture content (0.91%) showed about 70.42 (1.6 mol CO_2/kg). In contrast, the wet sample (2.35% water content) had a lower adsorption capacity than dry samples (0.91% water content) at equilibrium pressures below 2 MPa. This is likely due to the water content affecting bulk pore diffusion, the primary mode of adsorption mechanism at low pressures. The adsorption isotherm patterns of 18 ft. AB intact samples are presented in Fig. 6b. The sample showed an increased adsorption capacity than the sample with a much lower water content of 0.78% at elevated pressures of 3.6 MPa. The 18 ft. AB sample with 4.07% water content showed an adsorption capacity of 70.42 g/kg (1.6 mol of CO_2/kg) of coal and 0.78% water content exhibited an adsorption capacity of 48.41 g/kg (1.1 mol of CO_2/kg) of coal (Fig. 6b).

At increased pressures, the increased adsorption capacity of wet samples can be attributed to complex mechanisms such as CO_2 adsorption at water activated sites by expelling the adsorbed water (Day et al., 2008; Sun et al., 2016a) and mineralisation of CO_2. The observations made during the adsorption experiments with wet samples are represented in Fig. 7. After completing the adsorption-desorption tests on wet intact 18 ft. AB with water content 4.07%, the sample cell's bottom was found to be wet (Fig. 7a). The possible reason of water expulsion from the coal structure is that CO_2 can diffuse/dissolve into capillary water to access the coal matrix interior, causing the water molecules to desorb from the surfaces of nano, micro and mesopores (Fig. 7b - insert shows the image of nanosized pores and micro cleats found in the anthracite coal). This volume expulsion behaviour was previously reported in a study of CO_2 gas-water exchange experiments performed at pressures up to 4.5 MPa and temperatures up to 298.15 K (Sun et al., 2016a), which are similar to the parameters set up in the current investigation. With increasing CO_2 pressure, water molecules shift their contact angle and distribution, which in turn affects their adsorption capacity. Coal surfaces become hydrophobic, and the arrangements of water molecules are altered due to the increased H+ ion by CO_2's solubility. H_2O's interaction with coal weakens as the energy of van der Waals dispersive forces grows (Sun et al., 2018, 2022; Wiebe and Gaddy, 1940; Ibrahim and Nasr-El-Din, 2016). The present study's finding of enhanced adsorption is consistent with these prior findings.

The intact wet samples of both 9 ft. AB and 18 ft. AB anthracite coals had comparable isotherm patterns (Fig. 6a and b). However, the marginally enhanced adsorption capacity seen above 1 MPa equilibrium pressures with 9 ft. AB samples is correlated with the sample's low carbon content (89.5%) in comparison to 18 ft. AB (92.05%). The low carbon content coals contain higher polarised sites with functional and carbon containing groups where CO_2 and water molecules generally prefer to adsorb (Mahajan and Walker, 1971; Allardice and Evans, 1971; Nishino, 2001; Kadioğlu and Varamaz, 2003; Qi and LeVan, 2005; Miura et al., 2001; Day et al., 2008).

Fig. 6c compares the isotherm patterns of powdered 18 ft. AB coal samples with 0.78% and 1.2% water content. The adsorption capacity of the dry powdered sample was significantly greater than that of the wet samples. When the pressure was increased, the disparity in adsorption capacity grew. Powdered samples of 18 ft. AB with 0.78% water content adsorbed 66.02 g/kg (1.5 mol of CO_2/kg) of coal, while samples with 1.2% water content had an adsorption capacity of 44.41 (1.1 mol of CO_2/kg) of coal at 3.5 MPa, showing a 33% reduction in adsorption capacity (Fig. 6c). This pattern reflects the findings of Wang et al. (2011), who found that the amount of adsorbed CO_2 on wet coal samples was reduced by 69% when compared to dry powdered samples. The trends observed for the powdered samples (Fig. 6c) is expected as the adsorbed water forms hydrogen bonds with the polar functional group and carbon-containing groups of coal structure (Mahajan and Walker, 1971; Allardice and Evans, 1971; Nishino, 2001; Kadioğlu and Varamaz, 2003; Qi and LeVan, 2005; Miura et al., 2001). By pulverising the coal samples, these polarisation sites are exposed for water to absorb. Since H_2O molecules have a high heat of adsorption, it is difficult for CO_2 to replace the water molecules adsorbed on the polarised sites on the coal surface of the powdered samples (Day et al., 2008). This shows the effect of the pulverising the sample on adsorption capacity which may not represent the field conditions (Almolliyeh et al., 2023).

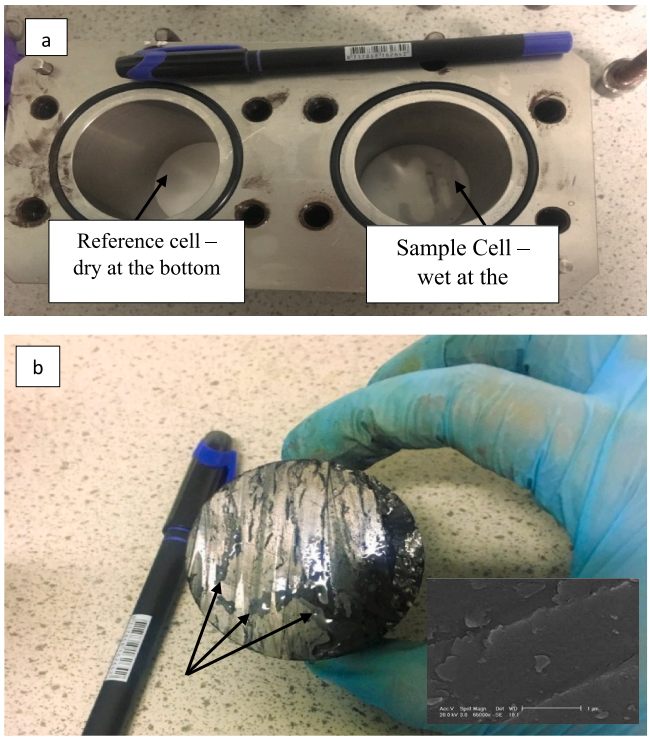

Fig. 7. Signs of residual water after CO_2 adsorption test on intact 18 ft. coal - a) at the bottom on the adsorption cell, b) at the bottom of the sample core (insert show the SEM images of nanosized fractures).

Fig. 6d depicts the CO_2 adsorption-desorption isotherms of powdered samples of 18 ft. AB coal with 0.78% and 1.2% water content. The isotherm patterns displayed the type II adsorption isotherm and H3 hysteresis pattern described by International Union of Pure and Applied Chemistry (IUPAC) (Sing et al., 1985; Thommes et al., 2015). The adsorption-desorption isotherm of sample with 0.78% water content showed clear hysteresis by exhibiting a positive deviation. The sample with 1.2% water content did not exhibit the substantial positive deviation at higher pressure (> 2 MPa). The reason for this could be that in wet samples, CO_2 must compete with water molecules at activated sites and be easily released from weakly adsorbed external sites at higher pressures (> 2 MPa). The CO_2 molecules adsorbing inside the narrow pores were not ready for desorption at lower pressure range (< 2 MPa) and reflected as hysteresis in the isotherm (Fig. 6d).

The calculated amount of CO_2 remain adsorbed at zero equilibrium pressure set up during desorption is referred to as residual CO_2. When

the residual amount of CO_2 on the powdered dry sample (0.78% water content) of 18 ft. AB coal was compared to the wet sample (1.2% water content) of 18 ft. AB coal, the dry sample had 1.18 mol/kg of coal retained at the end of desorption while the wet sample had 0.65 mol/kg coal retained in the coal. These findings support the discussion of less amount of CO_2 enter the nano/micropores that has been occupied by the water.

At lower and intermediate pressures (< 6.1 MPa), there was good agreement between experimental adsorption isotherms of intact samples and Langmuir model results (Figs. 6b and c). The experimental results deviated from the model to show the high-density adsorption build-up at high pressures (from 6.1 MPa to 6.4 MPa). This was evident in the intact samples of 18 ft. AB (0.78% water content) where high density CO_2 adsorption occurs within microfractures of intact coal (Figs. 6b) and fit very well with the BET model. However, at a similar pressure range, the experimental results of the powdered samples of 18 ft. AB with 0.78% and 1.2% water contents were in good agreement with the Langmuir model, indicating that water molecules adsorb on the exposed hydrophilic sites and prevent the high-density CO_2 adsorption (Fig. 6c), showing the influence of sample fabric and water. The BET model did not fit well with the powder samples of dry and wet 18 ft. AB (Fig. 6c). It is likely that the adsorbed water on the large surface area available for water molecules cannot be easily displaced by gas molecules, preventing the CO_2 access to the pores to form high dense layers. For a dry sample of 18 ft. AB (Fig. 6c), the lower density adsorbed phase on large, exposed surface area reflected on the isotherm and fitted better with the Langmuir model than that of BET, signifying the influence of sample fabric (Almolliyeh et al., 2023).

3.1.1. Water-coal interaction

The resulted adsorption capacities may not be occurred only by the physical gas adsorption on coal surface. Other factors such as physiochemical nature of water and biological conditions might have greater influence. The water wettability and capillary phenomena must be widely investigated for the water-coal-CO_2 system. The Fig. 8a shows the water holding capacity of the two coal samples (9 ft. AB intact and powder) at varying suction condition. According to Allardice et al. (2003), it has been observed that anthracite coals exhibit a lower degree of hydrophilicity compared to bituminous coal. The hydrophobic characteristics of anthracite coals are evident in their diminished water retention capacity. The investigation of the water retention characteristics of coal contributes to the advancement of knowledge regarding the long-term sequestration of CO_2 within coal deposits.

The chemical conditions of the retained water at high pressures can react with CO_2 and induce inorganic/biomineralization of CO_2. CO_2 reduces the water-wettability of coal and, as pressure increases, increases CO_2 solubility in water. This induces a low pH and the dissolution of inorganic salts, which destabilises the double layer surrounding the coal surface and renders it hydrophobic, thereby increasing CO_2 adsorption. The phenomenon of wettability in CO_2-coal-water is independent of coal rank (Ibrahim and Nasr-El-Din, 2016; Tokunaga and Wan, 2013; Sun et al., 2022).

The inorganic mineralisation phenomenon can be understood by the pH buffering capacity of the coal samples. The Fig. 8b shows the pH of the water samples were increased after equilibrating with coal because of the mineral dissolution. The concentrations of cations released from the coal during the equilibration indicate the possible dissolution of alkali minerals (example, dissolution of calcium increases alkalinity) from the coal surface. For example, carbonic acid (H_2CO_3) causes the pH 5.8 of the deionised water. After equilibrating with coal, the pH rises to 6.56 (Table 3). The measured cations concentration for the corresponding coal-water mix confirms the alkali mineral dissolution (Table 3) is the reason for the pH neutralisation. The dissolution of alkali minerals from coal was previously studied by Massarotto et al. (2010). Their results were similar to that obtained in this study. This clearly suggests that the released alkali minerals from the coal, particularly calcium, would interact with H_2CO_3 to precipitate as $CaCO_3$ and influence the CO_2 retention behaviour on coal.

3.1.2. Biofilm on coal surface

It has been hypothesized that surface biofilms on coal samples could trigger the biomineralization of carbon dioxide. The scanning electron microscope images of coal samples are shown in Fig. 9. Fig. 9a shows evidence of some biofilm on the surface cracks of the coal sample and naturally occurring bacteria can be seen. These images clearly show the presence of intact rod-shaped bacteria growing on small chunks of coal Fig. 9b. These bacteria likely belong to the genus *Bacillus*, which is often found in coal seams (Mitchell et al., 2008, 2009). To identify the bacteria found on the natural coal sample, the images were compared with SEM images of coal samples with laboratory grown *Bacillus mojavensis*. Bacteria was grown on the 9 ft. AB coal using laboratory procedure described in supplementary section. The scanning electron microscope images of the laboratory grown *Bacillus mojavensis* on 9 ft. AB coal sample is shown in Fig. 9c. The morphology of the bacteria in each set of

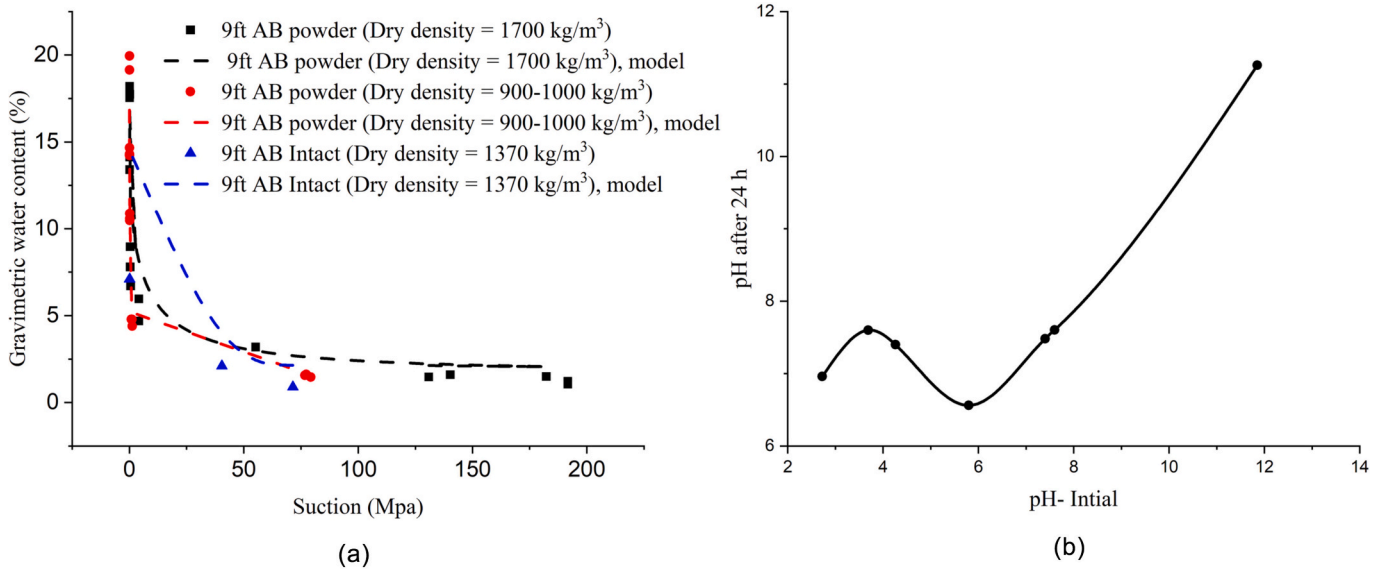

Fig. 8. (a) Water retention characteristics and (b) pH buffering capacity of 9 ft. AB coal.

Table 3
pH buffering capacity of 9 ft. Aberpergwm coal.

Initial pH	pH after 24 h	Ca (mg/g of coal)	Na (mg/g of coal)	K (mg/g of coal)	Mg (mg/g of coal)	Mn (mg/g of coal)	B (mg/g of coal)	Ba (mg/g of coal)
2.73	6.96	0.031	0.005	0.013	0.005	0.0004	0.0002	0.00009
3.69	7.6	0.018	0.004	0.01	0.002	0.0002	0.0002	0.00002
4.26	7.4	0.019	0.005	0.011	0.003	0.0002	0.0002	0.00036
5.8	6.56*	0.02	0.004	0.004	0.007	0.0003	0.0002	0.00001
11.85	11.26	0.001	**	0.012	0	0	0.0001	0.0002

* Natural pH with DI water, **NaOH is used for adjusting the pH.

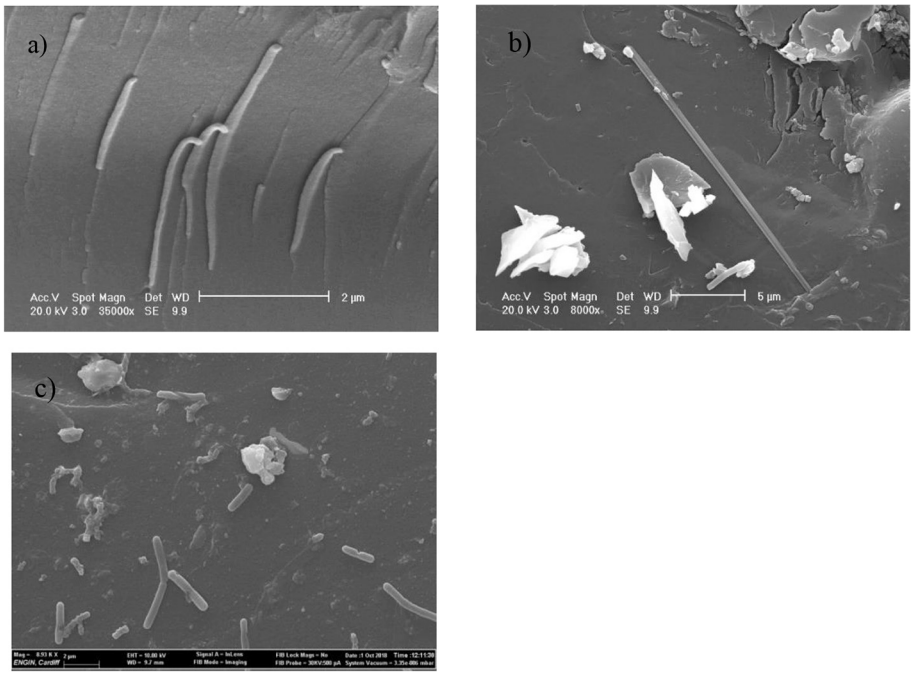

Fig. 9. Scanning electron photomicrographs of intact 9 ft Aberpergwm coal showing a) sign of biofilm on the surface cracks, b) rod-shaped species, similar to that of the genus Bacillus, and c) scanning electron photomicrographs of the laboratory grown bacteria on 9 ft Aberpergwm coal.

images were near-identical (Fig. 8). The typical length of *Bacillus mojavensis* cells is 2 µm to 4 µm and a width of 0.5 µm to 1 µm (Roberts et al., 1994). *Bacillus mojavensis* are commonly present in these types of samples and have been identified in previous works as particularly resilient to high pressure CO_2 (Mitchell et al., 2008, 2009).

3.2. CO_2 adsorption isotherms of caprock constituents

3.2.1. East Irish Sea rock samples

The manometric adsorption experiments were performed only on two rock samples due to the longer period to attain equilibrium for intact undisturbed samples. However, it has been previously documented in literatures that manometric set up can be used to measure the CO_2 adsorption capacity more accurately (Khosrokhavar et al., 2014). The East Irish Sea rock sample R1 (CaO = 20.25% and FeO = 4.9%) and R2 (CaO = 9.54% and FeO = 1.18%) were chosen for adsorption experiments due to their differences in calcium and iron content. The CO_2 adsorption isotherm pattern of the East Irish Sea rock samples is depicted in Fig. 10a. The rock sample R1 had a low adsorption capacity of 4.4 g/kg of rock (0.1 mol of CO_2/kg) up to an equilibrium pressure of 2 MPa and which increased to 39.61 g/kg (0.9 mol of CO_2/kg) of rock at an equilibrium pressure of 3.5 MPa (Fig. 10a). The rock sample R2 had a lower adsorption capacity of 1.23 g/kg (0.028 mol of CO_2/kg) of rock compared to R1 (Fig. 10a). When the pressure was increased, a clear Langmuir type isotherm pattern was observed. The CO_2 interaction with shale containing carbonate and pyrite minerals undergo dissolution reaction and forming secondary carbonate minerals (Montegrossi et al., 2022). This may be the possible reason that the rock sample R1 had a higher adsorption capacity compared to the rock sample R2.

Previous experiments in the subcritical range of CO_2 showed 3.18 g/kg (0.07 mol CO_2/kg) sandstone at 1 MPa equilibrium pressure and 21.18 g/kg (0.48 mol CO_2/kg) sandstone at 2 MPa equilibrium pressure (Tajnik et al., 2013), with the adsorption isotherm fitting very well to the Langmuir-type (monolayer) model (Jedli et al., 2016). Fakher and Imqam (2020) found that shale rocks could adsorb 16.72 g/kg (0.38 mol of CO_2/kg) of rock using a volumetric adsorption setup very similar to the one used in this study. More relevant to the coal seam context, the manometric adsorption experiments conducted with a carboniferous black shale from a depth of 745 m containing coal-associated sediments showed an adsorption capacity of 7.7 g of CO_2/kg of coal (Khosrokhavar et al., 2014). The leakage scenario must be site-specific, and the minerals from the overburden must be studied for their adsorption capacity. The adsorption capacity of sandstone rock samples, predominantly found above the coal seams focused on in the current study, to adsorb CO_2 varied with depth, clay content, mineral composition, water content, and biofilm content (Botan et al., 2010; McGrail et al., 2009; Kwak et al., 2011; Loring et al., 2011; Shao et al., 2011; Tokunaga and Wan, 2013; Kamihira et al., 1987; Enomoto et al., 1997; Zhang et al., 2006). Separate adsorption experiments were conducted on sand (dry, wet, and biofilm loaded), MX80 bentonite and Speswhite kaolinite samples to understand the adsorption behaviour of each mineral constituent in the sandstone, and the results are discussed in the subsequent section.

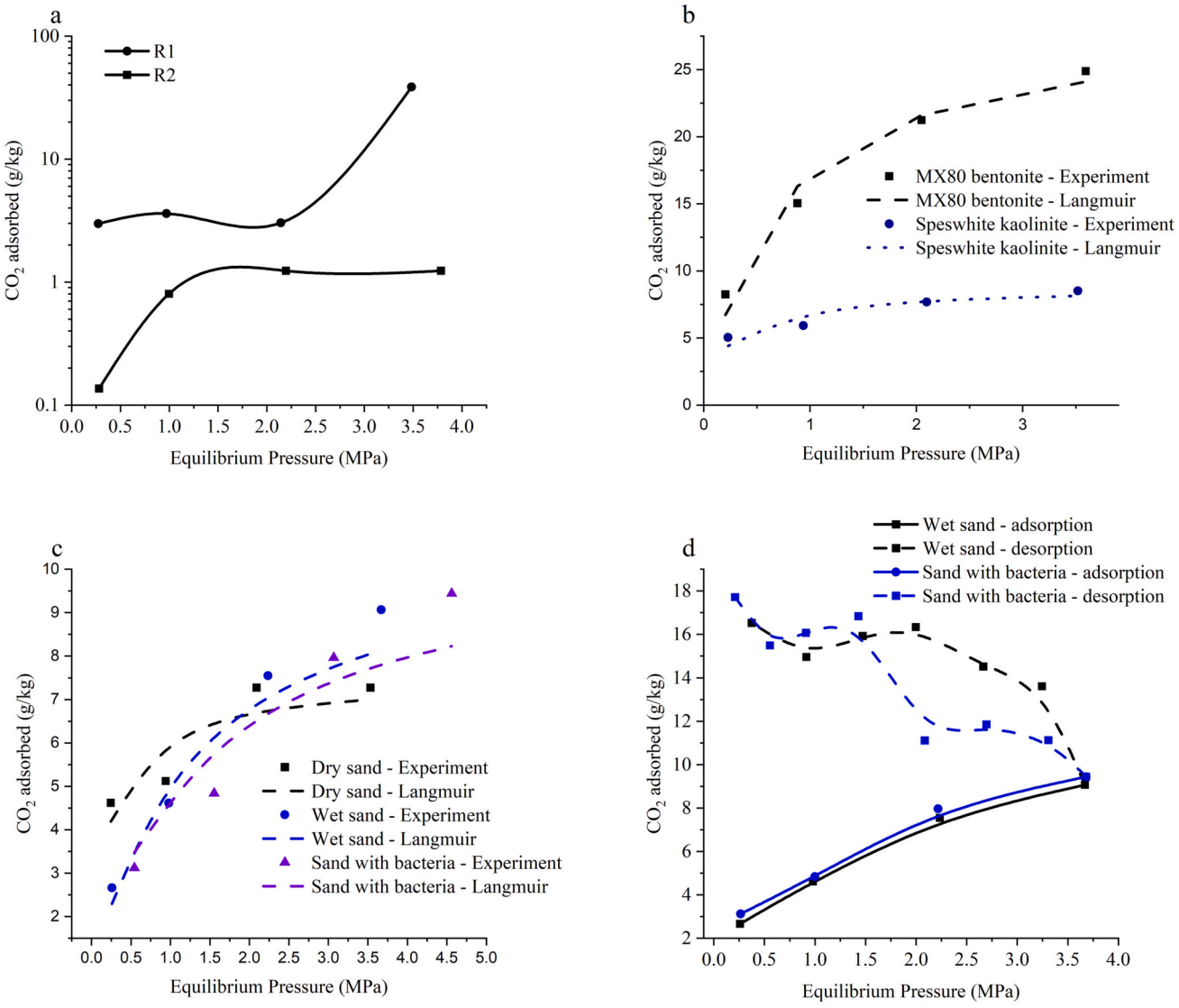

Fig. 10. (a) CO_2 adsorption isotherms of rock samples, (b) adsorption isotherms of clays, (c) dry sand, wet sand and sand with bacteria, and (d) adsorption-desorption isotherms of wet sand and sand with bacteria.

3.2.2. CO_2 adsorption on clay minerals, dry sand, wet sand, and sand loaded with Bacillus mojavensis

Fig. 10b shows the CO_2 adsorption isotherm pattern of MX80 bentonite and Speswhite kaolin. At an equilibrium pressure of 3.59 MPa, MX80 bentonite had a maximum CO_2 adsorption capacity of 24.65 g/kg (0.56 mol/kg (Fig. 10b). Jeon et al. (2014) reported a comparable adsorption capacity of about 26.41 (0.6 mol of CO_2/kg) of bentonite at an equilibrium pressure of 3.5 MPa. Previous studies reported an adsorption capacity ranging from 0.16 to 0.25 mol of CO_2/kg of Na-bentonite at equilibrium pressures (3.5 MPa) (Volzone, 2006). Previous studies have shown CO_2 molecules can penetrate the interlayer spacing of swelling clays (bentonite) and expand the basal spacing (Okolo et al., 2019; Loring et al., 2012; Ilton et al., 2012; Schaef et al., 2012). However, non-polar fluids such as CO_2 cannot simply replace the cations and expel the interlayer water but diffuse into the water to reach the interlayer space of the expanding clay minerals such as bentonite. The CO_2 adsorption mechanism on kaolinite was ascribed to CO_2 molecules adsorbing on the intragranular porosity and was characterised as physical sorption (Chen and Lu, 2015; Hu et al., 2019). Speswhite kaolin exhibited a maximum adsorption capacity of 8.36 g/kg (0.19 mol of CO_2/kg) of kaolinite at an equilibrium pressure range of 3.51 MPa (Fig. 10b). Volzone (2006) reported that the kaolinite mineral's maximum adsorption capacity was approximately 0.15 mol CO_2/kg of kaolinite, while Chen and Lu (2015) reported that Georgia kaolinite's maximum adsorption capacity was 0.3 mol CO_2/kg of kaolinite. The reported values were comparable to the current study's adsorption capacity value.

Bacillus mojavensis bacteria are native to sandstone rock strata and could affect the interaction of CO_2 with caprock (Mitchell et al., 2008; Mitchell et al., 2009; Peet et al., 2015). The *Bacillus mojavensis* type strain grows well in the CO_2-water-rock environment. The biofilms formed by *Bacillus mojavensis* are resilient to high-pressure CO_2 and can enhance the solubility trapping, mineralisation of CO_2 through ureolysis, and $CaCO_3$ precipitation. CO_2 gas adsorption tests were performed on *Bacillus mojavensis* loaded sand samples and compared to the dry and wet sand samples.

Fig. 10c shows the CO_2 adsorption and desorption isotherm patterns of dry sand, sand with water, sand with Nutrient Broth E and sand with bacteria, respectively. Dry sand showed a slightly reduced adsorption capacity (0.16 mol/kg) at a maximum equilibrium pressure of 3.5 MPa (Fig. 10c) than wet samples. Wet sand had a maximum adsorption capacity of about 0.2 mol of CO_2/kg (Fig. 10c). A control adsorption test was performed using Nutrient Broth *E*-loaded sand that had been used to grow *Bacillus mojavensis* bacteria and results are presented in the

supplementary section.

The maximum adsorption capacity of biofilm-loaded sand samples was 9.24 g/kg (0.21 mol /kg) (Fig. 10c). In comparison, the adsorption capacities of wet and biofilm-loaded sand samples were comparable (Fig. 10c). The dry sand showed lower capacity of 9.04 g/kg (0.16 mol/kg). The dry sand reached equilibrium around 2 MPa in the isotherm patterns shown in Fig. 10c, whereas the wet sand and biofilm-loaded sand showed a linear increase with pressure increase up to 3.5 MPa and 4 MPa equilibrium pressures, respectively.

Interestingly, the desorption pattern for *Bacillus mojavensis*-loaded sand demonstrated no discernible CO_2 gas desorption upon decreasing equilibrium pressure (Fig. 10d). on other hand, it displayed an increasing amount of CO_2 adsorbed. This behaviour demonstrates definitively that a significant portion of the 0.21 mol/kg biofilm-loaded sand may have been mineralized/chemisorbed, and that mineralisation or chemisorption occurs regardless of pressure. The adsorption-desorption experiment lasted 12 days in total and yielded an adsorption capacity of 17.6 g/kg (0.4 mol of CO_2) per kg of biofilm-coated sand specimen (Fig. 10d). A similar pattern was observed for sand with water (Fig. 10d) showed adsorption rather than desorption during the pressure step down desorption stages, indicating that water/biofilms may enhance solubility trapping of CO_2 (Mitchell et al., 2010). While dry sand contains a limited number of activated sites within the quartz nanopores, wet sand retains the CO_2 at the water activated hydrophilic sites in the quartz and fills the nanopores with increased density (Sun et al., 2016b).

3.2.3. Evaluation of CO_2 adsorption on rocks and clays using the Langmuir model

The Langmuir model was used to fit equilibrium CO_2 adsorption data obtained with dry sand, wet sand, sand with biofilm, MX80 bentonite and Speswhite kaolin (Langmuir, 1916, 1917, 1918). Figs. 10b represent the Langmuir adsorption isotherm model compared with experimental isotherms for MX80 bentonite and Speswhite kaolin. The experimental data of MX80 bentonite and Speswhite kaolin fit the Langmuir model very well (Fig. 10b). The Langmuir maximum adsorption capacity of MX80 bentonite was about 28.62 g/kg, and the Langmuir pressure b (half-loading pressure) was approximately 1.5×10^{-6} Pa^{-1} (Table 4). For a half-loading pressure of 4.53×10^{-6} Pa^{-1}, the Langmuir maximum adsorption capacity of the Speswhite kaolinite was approximately 8.64 g/kg of kaolinite (Table 4). The adsorption energy of MX80 bentonite was −23.31 kJ/mol and that of Speswhite kaolinite was −29.02 kJ/mol (Table 4).

Figs. 10c depict the experimental data fitted to the Langmuir model for dry sand, wet sand and sand with biofilm, respectively. The experimental data for dry sand agrees very well with the model, indicating that the sand has a limited number of available sites for CO_2 gas molecules and that the sites are saturated at around 2 MPa equilibrium pressure. Wet sand and *Bacillus mojavensis*-loaded sand, on the other hand, deviated from the model and increased linearly, indicating that more than one adsorption mechanism influences CO_2 adsorption on biofilm-loaded sand.

Table 4
Langmuir parameters and energy of adsorption obtained for dry, wet, *Bacillus mojavensis* loaded sand, MX80 bentonite and Speswhite kaolin.

Sample description	Langmuir pressure b (Pa^{-1})	Langmuir maximum adsorption capacity, m_∞, g of CO_2/kg of coal	ΔH_{ad} kJ/mol	ΔG^0_{ad} (kJ/mol)
Dry sand	5.39×10^{-6}	7.37	−29.84	−30.07
Sand with water	1.14×10^{-6}	10.08	−25.21	−33.93
Sand with *Bacillus mojavensis*	9.67×10^{-7}	10.08	−24.81	−34.32
MX80 bentonite	1.5×10^{-6}	28.62	−23.31	−33.24
Speswhite kaolin	4.53×10^{-6}	8.64	−29.02	−34.02

The Langmuir maximum adsorption capacities of the sand samples were approximately 7.37 g of CO_2/ kg of dry sand, 10.08 g of CO_2/ kg of wet sand, and 10.08 g of CO_2/ kg of *Bacillus mojavensis* loaded sand. The Langmuir pressures (*b*) were about 5.39×10^{-6} Pa^{-1} for dry sand, 1.14×10^{-6} Pa^{-1} for dry sand, 9.69×10^{-7} Pa^{-1} for dry sand (Table 4). While the current study only examined a restricted number of samples, the adsorption capacities of various rock types, including sandstone (3.2 g of CO_2/kg of coal), claystone-sandstone (11 g of CO_2/kg of coal), siltstone (12.4 g of CO_2/kg), siltstone, and limestone (1.6 g of CO_2/kg), extracted from the overburden of a coal mine in Slovenia (Tajnik et al., 2013), were found to be similar to the findings reported in the current study (refer to Table 4). In a study conducted by Zhang et al. (2018), it was observed that the adsorption of CO_2 on quartz crystals followed a Langmuir-type adsorption behaviour. Furthermore, molecular simulations performed by Carchini et al. (2020) demonstrated that the adsorption of CO_2 on the quartz surface is of a physical nature. In a simulation study (Yang et al., 2022), the energy of physical adsorption on the sand was given as 22 kJ/mol, which is comparable to the adsorption energy calculated in the current study (29.8 kJ/mol for the dry sand: Table 4).

3.3. Limitations and uncertainties

The current study's sample size is not exhaustive, and sample sizes may cause uncertainty in the study's results. Biological effects, for example, are very small, and such small effects cannot be statistically represented by small samples. As a result, geomaterials with varying biogeochemical conditions are proposed to provide a comprehensive data set. However, the current study's samples were chosen to mimic the similar coal bearing strata of the coal samples chosen from and relevant. The adsorption pressure data deviating from the pressure measurement transducers were plotted against a secondary transducer fitted in the measurement cell with a ± 15 Pa deviation uncertainty for any experiment conducted up to 6.5 MPa for the validity and data acceptance of the smaller sample size. The adsorption capacity data yielded in this study were comparable to previously documented research.

3.4. Implications for current knowledge of geological CO_2 sequestration

One of the goals of CO_2 sequestration in geological formations is to retrofit existing and decommissioned coal mines/coal seams as CO_2 storage units with the possibility of extracting coal bed methane (CBM). Recent developments in CO_2 sequestration in coal seams have focused on the operational and technical feasibility of new potential engineering practises such as horizontal well injection to improve CO_2-coal contact area and injectivity (ROCCS Project, 2023). Laboratory-measured adsorption capacity can be used to determine the potential of these engineering practises. The current study's findings have an impact on current research focused on European coal seams by feeding adsorption capacity data of geomaterials to large-scale ex-situ experiments and in-situ pilot-scale studies testing the CO_2-CBM.

4. Conclusions

This work comprehensively presented the CO_2 adsorption on geomaterials in the perspective of CO_2 storage in coal seams. Wet coal samples of intact samples showed lower adsorption capacity than the lower moisture content sample at lower pressure range of the subcritical region (<1 MPa). At elevated pressures (up to 6.4 MPa) the comparable adsorption capacity of the wet and dry samples was attributed to the volume expulsion, water mineralisation and biomineralization of CO_2. However, the wet powdered samples showed lower adsorption capacity as the water molecules at the exposed hydrophilic sites were not easily

desorbed by CO_2. Moreover, pulverising the samples may expose more polarising sites and favours H_2O adsorption than CO_2. The Langmuir and BET isotherm model predictions supported the interpretations. The supporting experiments such as water retention characteristics of the coal samples, pH buffering capacity of the coal showed that the inorganic and biomineralization cannot be ignored.

The adsorption experiments dry, wet sand and biofilm-laden sand samples showed that the biogeological condition of the caprock system has greater influence on the adsorption properties. The influence of the East Irish Sea's inorganic mineral composition on CO_2 adsorption capacity was evident, as documented in previous studies. The adsorption-desorption isotherms of biofilm-loaded sand revealed that CO_2 adsorbs independently of CO_2 concentration in the gas phase (equilibrium pressure), indicating chemisorption. This work also given insights to explore the possibilities of sequestering CO_2 in biomass filled voids of disused coal mines.

This work comprehensively presented the CO_2 adsorption on geomaterials in the perspective of CO_2 storage in coal seams. Comparatively, the adsorption capacities of the geomaterials tested in the study is smaller than the coal samples. However, it has been shown that the influence of the biogeological conditions of the coal seams and the cape rock system cannot be ignored.

CRediT authorship contribution statement

Maram Almolliyeh: Conceptualization, Methodology, Validation, Investigation, Data curation, Writing – original draft, Writing – review & editing. **Snehasis Tripathy:** Supervision, Project administration, Resources, Writing – review & editing. **Sivachidambaram Sadasivam:** Conceptualization, Methodology, Formal analysis, Writing – review & editing. **Shakil Masum:** Conceptualization, Methodology, Writing – review & editing. **Sara Edwards Rassner:** Investigation, Data curation, Writing – review & editing. **Andy Mitchell:** Supervision, Project administration, Funding acquisition. **Hywel Rhys Thomas:** Supervision, Project administration, Funding acquisition.

Declaration of Competing Interest

The authors confirm that there are no known conflicts of interest associate with this research article.

Data availability

Data will be made available on request.

Acknowledgement

The research was performed as part of the Sêr Cymru- Low Carbon Energy and Environment Research Network Wales project, which was part funded by the European Regional Development Fund, through the Welsh Government. The authors are thankful to the funding agency. The authors are grateful to British Geological Survey (BGS) for providing the East Irish Sea Rock samples. Also, the authors appreciate the help of to our research technicians Anthony Oldroyd and Malcolm Seaborne for their time and effort to run the high-pressure adsorption experiments. We appreciate Steven Rankmore, our technician, for extracting coal core samples.

Appendix A. Supplementary data

Supplementary data to this article can be found online at https://doi.org/10.1016/j.coal.2023.104340.

References

Allardice, D.J., Evans, D.G., 1971. The-brown coal/water system: part 2. Water sorption isotherms on bed-moist Yallourn brown coal. Fuel 50 (3), 236–253. https://doi.org/10.1016/0016-2361(71)90014-7.

Allardice, D.J., Clemow, L.M., Favas, G., Jackson, W.R., Marshall, M., Sakurovs, R., 2003. The characterisation of different forms of water in low rank coals and some hydrothermally dried products. Fuel 82 (6), 661–667. https://doi.org/10.1016/S0016-2361(02)00339-3.

Almolliyeh, M., Tripathy, S., Sadasivam, S., Masum, S., Thomas, H.R., 2023. Effect of physical nature (intact and powder) of coal on CO_2 adsorption at the subcritical pressure range (up to 6.4 MPa at 298.15 K). ACS Omega 8 (7), 7070–7084. https://doi.org/10.1021/acsomega.2c0794.

Botan, A., Rotenberg, B., Marry, V., Turq, P., Noetinger, B., 2010. Carbon dioxide in montmorillonite clay hydrates: thermodynamics, structure, and transport from molecular simulation CORE view metadata, citation and similar papers at core. J. Phys. Chem. C 35, 14962. Available at: https://hal.archives-ouvertes.fr/hal-00531724.

Brunauer, S., Emmett, P.H., Teller, E., 1938. Adsorption of Gases in Multimolecular Layers. Available at: https://pubs.acs.org/sharingguidelines.

Carchini, G., Hussein, I., Al-Marri, M.J., Shawabkeh, R., Mahmoud, M., Aparicio, S., 2020. A theoretical study of gas adsorption on α-quartz (001) for CO_2 enhanced natural gas recovery. Appl. Surf. Sci. 525 https://doi.org/10.1016/j.apsusc.2020.146472.

Charrière, D., Behra, P., 2010. Water sorption on coals. J. Colloid Interface Sci. 344 (2), 460–467. Available at: https://doi.org/10.1016/j.jcis.2009.11.064.

Chen, Y.H., Lu, D.L., 2015. CO_2 capture by kaolinite and its adsorption mechanism. Appl. Clay Sci. 104, 221–228. https://doi.org/10.1016/J.CLAY.2014.11.036.

Dai, Z., Ronholm, J., Tian, Y., Sethi, B., Cao, X., 2016. Sterilization techniques for biodegradable scaffolds in tissue engineering applications. J. Tissue Eng. 7 https://doi.org/10.1177/2041731416648810.

Day, S., Sakurovs, R., Weir, S., 2008. Supercritical gas sorption on moist coals. Int. J. Coal Geol. 74 (3–4), 203–214. https://doi.org/10.1016/j.coal.2008.01.003.

Depaolo, D.J., Cole, D.R., 2013. Geochemistry of geologic carbon sequestration: An overview. Rev. Mineral. Geochem. 77, 1–14. Available at: https://doi.org/10.2138/rmg.2013.77.1 [Accessed: 12 March 2019].

Doner, H.E., Lynn, W.C., 1989. Carbonate, Halide, Sulfate, and Sulfide Minerals. In: Dixon, J.B., Weed, S.B. (Eds.), Minerals in Soil Environments. https://doi.org/10.2136/sssabookser1.2ed.c6.

Elliott, J., Lira, C., 2012. Introductory Chemical Engineering Thermodynamics. Prentice Hall, Upper Saddle River, NJ.

Enomoto, A., Nakamura, K., Nagai, K., Hashimoto, T., Hakoda, M., 1997. Inactivation of food microorganisms by high-pressure carbon dioxide treatment with or without explosive decompression. Biosci. Biotechnol. Biochem. 61 (7), 1133–1137. Available at: https://academic.oup.com/bbb/article/61/7/1133/5947318.

Fakher, S., Imqam, A., 2020. High pressure-high temperature carbon dioxide adsorption to shale rocks using a volumetric method. Int. J. Greenhouse Gas Control 95. https://doi.org/10.1016/j.ijggc.2020.102998. Available at:

Guo, J., Zhai, Z., Wang, L., Wang, Z., Wu, J., Zhang, B., Zhang, J., 2017. Dynamic and thermodynamic mechanisms of TFA adsorption by particulate matter. Environ. Pollut. 225, 175–183. Available at: https://doi.org/10.1016/j.envpol.2017.03.049.

Hu, X., Deng, H., Lu, C., Tian, Y., Jin, Z., 2019. Characterization of CO_2/CH_4 Competitive Adsorption in various Clay Minerals in Relation to Shale Gas Recovery from Molecular simulation. Energy Fuel 33 (9), 8202–8214. Available at: https://doi.org/10.1021/acs.energyfuels.9b01610.

Hu, A., Zhang, Y., Xiong, P., Yang, Y., Liu, Z., 2020. Kinetic characteristics and modeling comparison of methane adsorption on gas shale. Energy Sourc. Part A: Recov. Util. Environ. Effects 00 (00), 1–15. Available at: https://doi.org/10.1080/15567036.2020.1849461.

Ibrahim, A.F., Nasr-El-Din, H.A., 2016. Effect of water salinity on coal wettability during CO_2 sequestration in coal seams. Energy Fuel 30, 7532. https://doi.org/10.1021/acs.energyfuels.6b01205.

Ilton, E.S., Schaef, H.T., Qafoku, O., Rosso, K.M., Felmy, A.R., 2012. In situ X-ray diffraction study of Na+ saturated montmorillonite exposed to variably wet super critical CO_2. Environ. Sci. Technol. 46 (7), 4241–4248. https://doi.org/10.1021/es300234v.

Jedli, H., Jbara, A., Hedfi, H., Bouzgarrou, S., Slimi, K., 2016. Carbon dioxide adsorption isotherm study on various cap rocks in a batch reactor for CO_2 sequestration processes. Appl. Clay Sci. 136, 199–207. Available at: https://doi.org/10.1016/j.clay.2016.11.022.

Jeon, P.R., Choi, J., Yun, T.S., Lee, C.H., 2014. Sorption equilibrium and kinetics of CO_2 on clay minerals from subcritical to supercritical conditions: CO_2 sequestration at nanoscale interfaces. Chem. Eng. J. 255, 705–715. https://doi.org/10.1016/J.CEJ.2014.06.090.

Kadioğlu, Y., Varamaz, M., 2003. The effect of moisture content and air-drying on spontaneous combustion characteristics of two Turkish lignites. Fuel 82 (13), 1685–1693. https://doi.org/10.1016/S0016-2361(02)00402-7.

Kamihira, M., Taniguchi, M., Kobayashi, T., 1987. Sterilization of microorganisms with supercritical carbon dioxide. Agric. Biol. Chem. 51 (2), 407–412. https://doi.org/10.1080/00021369.1987.10868053.

Keller, J.U., Staudt, R., 2005. Gas adsorption equilibria: Experimental methods and adsorptive isotherms. In: Gas Adsorption Equilibria: Experimental Methods and Adsorptive Isotherms, pp. 1–422. Available at: http://ebooks.kluweronline.comhttp//www.springeronline.com.

Kerisit, S., Weare, J.H., Felmy, A.R., 2012. Structure and Dynamics of Forsterite-scCO_2/H_2O Interfaces as a Function of Water Content. Geochim. Cosmochim. Acta 84, 137–151. https://doi.org/10.1016/J.GCA.2012.01.038.

Khosrokhavar, R., Wolf, K.H., Bruining, H., 2014. Sorption of CH4 and CO_2 on a carboniferous shale from Belgium using a manometric setup. Int. J. Coal Geol. 128–129, 153–161. https://doi.org/10.1016/j.coal.2014.04.014.

Krooss, B.M., Van Bergen, F., Gensterblum, Y., Siemons, N., Pagnier, H.J.M., David, P., 2002. High-pressure methane and carbon dioxide adsorption on dry and moisture-equilibrated Pennsylvanian coals. Int. J. Coal Geol. https://doi.org/10.1016/S0166-5162(02)00078-2.

Kwak, J.H., et al., 2011. The role of H_2O in the carbonation of forsterite in supercritical CO_2. Int. J. Greenhouse Gas Control 5 (4), 1081–1092. https://doi.org/10.1016/J.IJGGC.2011.05.013.

Langmuir, I., 1915. Chemical reactions at low pressures. J. Am. Chem. Soc. 37 (5), 1139–1167. https://doi.org/10.1021/ja02170a017.

Langmuir, I., 1916. The constitution and fundamental properties of solids and liquids. Part I. Solids. J. Am. Chem. Soc. 38 (11), 2221–2295. Available at: https://doi.org/10.1021/ja02268a002.

Langmuir, I., 1917. The constitution and fundamental properties of solids and liquids. II. Liquids. J. Am. Chem. Soc. 39 (9), 1848–1906. Available at: https://doi.org/10.1021/ja02254a006.

Langmuir, I., 1918. The adsorption of gases on plane surfaces of glass, mica and platinum. J. Am. Chem. Soc. 40 (9), 1361–1403. https://doi.org/10.1021/ja02242a004.

Lavalleur, H.J., Colwell, F.S., 2013. Microbial characterization of basalt formation waters targeted for geological carbon sequestration. FEMS Microbiol. Ecol. 85 (1), 62–73. Available at: https://academic.oup.com/femsec/article/85/1/62/573693.

Loring, J.S., et al., 2011. In situ infrared spectroscopic study of forsterite carbonation in wet supercritical CO_2. Environ. Sci. Technol. 45 (14), 6204–6210. Available at: https://pubs.acs.org/sharingguidelines.

Loring, J.S., et al., 2012. In situ molecular spectroscopic evidence for CO_2 intercalation into montmorillonite in supercritical carbon dioxide. Langmuir 28 (18), 7125–7128. https://doi.org/10.1021/la301136w.

Mahajan, O.P., Walker, P.L., 1971. Water adsorption on coals. Fuel 50 (3), 308–317. https://doi.org/10.1016/0016-2361(71)90019-6.

Malani, A., Ayappa, K.G., 2009. Adsorption Isotherms of Water on Mica: Redistribution and Film Growth. J. Phys. Chem. B 113 (4), 1058–1067. Available at: https://doi.org/10.1021/jp805730p.

Massarotto, P., Golding, S.D., Bae, J.S., Iyer, R., Rudolph, V., 2010. Changes in reservoir properties from injection of supercritical CO_2 into coal seams - a laboratory study. Int. J. Coal Geol. 82 (3–4), 269–279. https://doi.org/10.1016/J.COAL.2009.11.002.

McGrail, B.P., Schaef, H.T., Glezakou, V.A., Dang, L.X., Owen, A.T., 2009. Water reactivity in the liquid and supercritical CO_2 phase: has half the story been neglected? Energy Procedia 1 (1), 3415–3419. https://doi.org/10.1016/J.EGYPRO.2009.02.131.

Mitchell, A.C., Phillips, A.J., Hamilton, M.A., Gerlach, R., Hollis, W.K., Kaszuba, J.P., Cunningham, A.B., 2008. Resilience of planktonic and biofilm cultures to supercritical CO_2. J. Supercrit. Fluids 47 (2), 318–325. Available at: https://linkinghub.elsevier.com/retrieve/pii/S0896844608002040.

Mitchell, A.C., Phillips, A.J., Hiebert, R., Gerlach, R., Spangler, L.H., Cunningham, A.B., 2009. Biofilm enhanced geologic sequestration of supercritical CO_2. Int. J. Greenhouse Gas Control 3 (1), 90–99. https://doi.org/10.1016/j.ijggc.2008.05.002.

Mitchell, A.C., Dideriksen, K., Spangler, L.H., Cunningham, A.B., Gerlach, R., 2010. Microbially enhanced carbon capture and storage by mineral-trapping and solubility-trapping. Environ. Sci. Technol. 44 (13), 5270–5276. https://doi.org/10.1021/es903270w.

Miura, K., Mae, K., Li, W., Kusakawa, T., Morozumi, F., Kumano, A., 2001. Estimation of Hydrogen Bond distribution in coal through the Analysis of OH stretching Bands in Diffuse Reflectance infrared Spectrum measured by in-Situ Technique. Energy Fuel 15 (3), 599–610. https://doi.org/10.1021/ef0001787.

Montegrossi, G., Cantucci, B., Piochi, M., Fusi, L., Misnan, M.S., Rashidi, M.R.A., Abu Bakar, Z.A., Tuan Harith, Z.Z., Bahri, N.H.S., Hashim, N., 2022. CO_2 reaction-diffusion experiments in shales and carbonates. Minerals 13, 56.

Morozova, D., Wandrey, M., Alawi, M., Zimmer, M., Vieth, A., Zettlitzer, M., Würdemann, H., 2010. Monitoring of the microbial community composition in saline aquifers during CO_2 storage by fluorescence in situ hybridisation. Int. J. Greenhouse Gas Control 4 (6), 981–989. https://doi.org/10.1016/J.IJGGC.2009.11.014.

Mukherjee, M., Misra, S., 2018. A review of experimental research on Enhanced Coal Bed methane (ECBM) recovery via CO_2 sequestration. Earth Sci. Rev. 179 (March), 392–410. Available at: https://doi.org/10.1016/j.earscirev.2018.02.018.

Murata, S., Hosokawa, M., Kidena, K., Nomura, M., 2000. Analysis of oxygen-functional groups in brown coals. Fuel Process. Technol. 67 (3), 231–243. https://doi.org/10.1016/S0378-3820(00)00102-8.

Myers, A.L., Monson, P.A., 2014. Physical adsorption of gases: the case for absolute adsorption as the basis for thermodynamic analysis. Adsorption 20 (4), 591–622. https://doi.org/10.1007/s10450-014-9604-1.

Nishino, J., 2001. Adsorption of water vapor and carbon dioxide at carboxylic functional groups on the surface of coal. Fuel 80 (5), 757–764. Available at: www.elsevier.com/locate/fuel.

Okolo, G.N., Everson, R.C., Neomagus, H.W.J.P., Sakurovs, R., Grigore, M., Bunt, J.R., 2019. Dataset on the carbon dioxide, methane and nitrogen high-pressure sorption properties of South African bituminous coals. In: Data in Brief, 25, p. 104248. https://doi.org/10.1016/J.DIB.2019.104248 [Accessed: 21 August 2019].

Ozdemir, E., Schroeder, K., 2009. Effect of Moisture on Adsorption Isotherms and Adsorption Capacities of CO2 on Coals. Energy Fuels 23 (5), 2821–2831.

Peet, K.C., Adam, J.E.F., Hernandez, H.H., Britto, V., Boreham, C., Ajo-Franklin, J.B., Thompson, J.R., 2015. Microbial growth under supercritical CO_2. Appl. Environ. Microbiol. 81 (8), 2881–2892. https://doi.org/10.1128/AEM.03162-14.

Pone, J.D.N., Halleck, P.M., Mathews, J.P., 2009. Sorption capacity and sorption kinetic measurements of CO_2 and CH_4 in confined and unconfined bituminous coal. Energy Fuel 23 (9), 4688–4695. https://doi.org/10.1021/ef9003158.

Qi, N., LeVan, M.D., 2005. Adsorption equilibrium modeling for water on activated carbons. Carbon 43 (11), 2258–2263. https://doi.org/10.1016/J.CARBON.2005.03.040.

Rahaman, A., Grassian, V.H., Margulis, C.J., 2008. Dynamics of water adsorption onto a calcite surface as a function of relative humidity. J. Phys. Chem. C 112 (6), 2109–2115. https://doi.org/10.1021/JP077594D.

Roberts, M.S., Nakamura, L.K., Cohan, F.M., 1994. Bacillus mojavensis sp. nov., distinguishable from Bacillus subtilis by sexual isolation, divergence in DNA sequence, and differences in fatty acid composition. Int. J. Syst. Bacteriol. 44 (2), 256–264. Available at: https://pubmed.ncbi.nlm.nih.gov/8186089/.

ROCCS Project, 2023. roccsproject.com. Accessed on 19 August 2023.

Sadasivam, S., Thomas, H.R., Zagorščak, R., Davies, T., Price, N., 2019. Baseline geochemical study of the Aberpergwm mining site in the South Wales Coalfield. J. Geochem. Explor. 202, 100–112. https://doi.org/10.1016/j.gexplo.2019.03.006.

Schaef, H.T., Ilton, E.S., Qafoku, O., Martin, P.F., Felmy, A.R., Rosso, K.M., 2012. In situ XRD study of Ca_2+ saturated montmorillonite (STX-1) exposed to anhydrous and wet supercritical carbon dioxide. Int. J. Greenhouse Gas Control 6, 220–229. https://doi.org/10.1016/j.ijggc.2011.11.001.

Shao, H., Ray, J.R., Jun, Y.-S., 2011. Effects of salinity and the extent of water on supercritical CO_2-induced phlogopite dissolution and secondary mineral formation. Environ. Sci. Technol. 45, 1737–1743. Available at: https://pubs.acs.org/sharinguidelines [Accessed: 5 May 2022].

Sing, K.S.W., Everett, D.H., Haul, R.A.W., et al., 1985. Reporting physisorption data for gas/solid systems with special reference to the determination of surface area and porosity. Pure Appl. Chem. 57 (4), 603–619.

Stach, E., Chandra, D., Taylor, G.H., Teichmuller, R.M.T., Mackowsky, M., 1982. Stach's Textbook Coal Petrology Stach. Available at: https://books.google.com/books/about/Stach_s_Textbook_of_Coal_Petrology.html?id=5cb3AAAAIAAJ.

Sun, H., Sun, W., Zhao, H., Sun, Y., Zhang, D., Qi, X., Li, Y., 2016a. Adsorption properties of CH4 and CO_2 in quartz nanopores studied by molecular simulation. RSC Adv. 6 (39), 32770–32778. https://doi.org/10.1039/c6ra05083b.

Sun, X., Yao, Y., Liu, D., Elsworth, D., Pan, Z., 2016b. Interactions and exchange of CO_2 and H2O in coals: An investigation by low-field NMR relaxation. Sci. Rep. 6 https://doi.org/10.1038/srep19919.

Sun, X., Yao, Y., Liu, D., Zhou, Y., 2018. Investigations of CO_2-water wettability of coal: NMR relaxation method. Int. J. Coal Geol. 188, 38–50. ISSN 0166-5162,. https://doi.org/10.1016/j.coal.2018.01.015.

Sun, X., Yao, Y., Liu, D., Elsworth, D., 2022. How does CO_2 adsorption alter coal wettability? Implications for CO_2 geo-sequestration. J. Geophys. Res. Solid Earth 127. https://doi.org/10.1029/2021JB023723 e2021JB023723.

Tajnik, T., Bogataj, L.K., Jurač, E., Lasnik, C.R., Likar, J., Debelak, B., 2013. Investigation of adsorption properties of geological materials for CO_2 storage. Int. J. Energy Res. 37 (8), 952–958. https://doi.org/10.1002/er.2901.

Thommes, M., Kaneko, K., Neimark, A., v., Olivier, J.P., Rodriguez-Reinoso, F., Rouquerol, J. and Sing, K.S.W., 2015. Physisorption of gases, with special reference to the evaluation of surface area and pore size distribution (IUPAC Technical Report). Pure Appl. Chem. 87 (9–10), 1051–1069. https://doi.org/10.1515/pac-2014-1117.

Tokunaga, Tetsu K., Wan, Jiamin, 2013. Capillary pressure and mineral wettability influences on reservoir CO_2 capacity. Rev. Mineral. Geochem. 77 (1), 481–503. https://doi.org/10.2138/rmg.2013.77.14.

Volzone, C., 2006. Retention of pollutant gases: Comparison between clay minerals and their modified products. Appl. Clay Sci. 36 (1–3), 191–196. https://doi.org/10.1016/J.CLAY.2006.06.013.

Wang, L., Zhang, M., Redfern, S.A.T., 2003. Infrared Study of CO_2 Incorporation into Pyrophyllite [$Al2Si4O10(OH)_2$] during Dehydroxylation. Clay Clay Miner. 51 (4), 439–444. Available at: https://doi.org/10.1346/CCMN.2003.0510410 [Accessed: 6 May 2022].

Wang, S., Elsworth, D., Liu, J., 2011. Permeability evolution in fractured coal: the roles of fracture geometry and water-content. Int. J. Coal Geol. 87 (1), 13–25. https://doi.org/10.1016/j.coal.2011.04.009.

Wang, L., Chen, E. Tao, Liu, S., Cheng, Y. Ping, Cheng, L. Biao, Chen, M. Yi, Guo, H. Jun, 2017. Experimental study on the effect of inherent moisture on hard coal adsorption–desorption characteristics. Adsorption 23 (5), 723–742. Available at: https://doi.org/10.1007/s10450-017-9889-y.

Wensink, E.J.W., Hoffmann, A.C., Apol, M.E.F., Berendsen, H.J.C., 2000. Properties of adsorbed water layers and the effect of adsorbed layers on interparticle forces by liquid bridging. Langmuir 16 (19), 7392–7400. https://doi.org/10.1021/la000009e.

White, C.M., Smith, D.H., Jones, K.L., Goodman, A.L., Jikich, S.A., Lacount, R.B., Dubose, S.B., Ozdemir, E., Morsi, B.I., Schroeder, K.T., 2005. Sequestration of carbon dioxide in coal with enhanced coalbed methane recovery: a review. Energy Fuel 19 (3), 659. https://doi.org/10.1021/ef040047w.

Wiebe, B.Y., Gaddy, V.L., 1940. The solubility of carbon dioxide in water at various temperatures from 12 to 40° and at pressures to 500 atmospheres. J. Am. Chem. Soc. 62, 815–817.

Yang, N., Yang, X., 2011. Molecular Simulation of Swelling and Structure for Na-Wyoming Montmorillonite in Supercritical CO2, 37(13), pp. 1063–1070. Available at: https://doi.org/10.1080/08927022.2010.547939.

Yang, X., et al., 2022. Correction of gas adsorption capacity in quartz nanoslit and its application in recovering shale gas resources by CO2 injection: a molecular simulation. Energy 240. https://doi.org/10.1016/j.energy.2021.122789.

Zhang, J., Davis, T.A., Matthews, M.A., Drews, M.J., LaBerge, M., An, Y.H., 2006. Sterilization using high-pressure carbon dioxide. J. Supercrit. Fluids 38 (3), 354–372. https://doi.org/10.1016/j.supflu.2005.05.005.

Zhang, Y., et al., 2018. Nanoscale rock mechanical property changes in heterogeneous coal after water adsorption. Fuel 218, 23–32. Available at: https://doi.org/10.1016/j.fuel.2018.01.006 [Accessed: 5 May 2022].

Zhang, X., Ranjith, P.G., Lu, Y., Ranathunga, A.S., 2019. Experimental investigation of the influence of CO_2 and water adsorption on mechanics of coal under confining pressure. Int. J. Coal Geol. 209, 117–129. https://doi.org/10.1016/j.coal.2019.04.004.

Zhang, J., Hu, Q., Chang, X., Qin, Z., Zhang, X., Marsh, S., Grebby, S., Agarwal, V., 2022. Water Saturation and distribution Variation in Coal Reservoirs: Intrusion and Drainage experiments using One- and Two-Dimensional NMR Techniques. Energy Fuel 36 (12), 6130–6143. https://doi.org/10.1021/acs.energyfuels.2c00592.